AGU PUBLICATIONS

Geophysical Research Letters

RESEARCH LETTER
10.1002/2016GL069558

Key Points:
- Subglacial bed forms (ribbed/rogen moraines, drumlins, and MSGL) are modeled
- Requisite mechanisms include down- and cross-ice till deformation and entrainment
- Ice speed and sediment thickness control subglacial bed form morphology

Supporting Information:
- Supporting Information S1
- Movie S1
- Movie S2
- Movie S3
- Table S1
- Table S1

Correspondence to:
T. E. Barchyn,
tbarchyn@gmail.com

Citation:
Barchyn, T. E., T. P. F. Dowling, C. R. Stokes, and C. H. Hugenholtz (2016), Subglacial bed form morphology controlled by ice speed and sediment thickness, *Geophys. Res. Lett.*, *43*, 7572–7580, doi:10.1002/2016GL069558.

Received 9 MAR 2016
Accepted 8 JUL 2016
Accepted article online 18 JUL 2016
Published online 30 JUL 2016

Subglacial bed form morphology controlled by ice speed and sediment thickness

Thomas E. Barchyn[1], Thomas P. F. Dowling[2], Chris R. Stokes[3], and Chris H. Hugenholtz[1]

[1]Department of Geography, University of Calgary, Calgary, Alberta, Canada, [2]Department of Geology, Lund University, Lund, Sweden, [3]Department of Geography, Durham University, Durham, UK

Abstract Subglacial bed forms (drumlins, ribbed moraines, and megascale glacial lineations) are enigmatic repetitive flow-parallel and flow-transverse landforms common in glaciated landscapes. Their evolution and morphology are a potentially powerful constraint for ice sheet modeling, but there is little consensus on bed form dynamics or formative mechanisms. Here we explore shallow sediment bed form dynamics via a simple model that iterates (i) down-flow till flux, (ii) pressure gradient-driven till flux, and (iii) entrainment and deposition of sediment. Under various boundary conditions, replicas of subglacial bed forms readily emerge. Bed form dynamics mirror those in subaqueous and aeolian domains. Transitions between ribbed moraines and elongate flow-parallel bed forms are associated with increasing ice speeds and declining sediment thickness. These simulations provide quantitative flux estimates and suggest that widely observed transitions in shallow sediment subglacial bed forms (e.g., ribbed moraines to drumlinoids to megascale glacial lineations) are manifestations of subtle variations in ice velocity and sediment thickness.

1. Introduction

Subglacial bed forms form ubiquitously in glaciated terrain (≈10% of Earth land surface) and are manifested as vast fields of repetitive streamlined hills and ridges. Bed forms range from flow-perpendicular sinuous ridges (termed ribbed or rogen moraines [*Dunlop and Clark*, 2006]), to flow-parallel bumps and ridges (termed drumlins [*Clark et al*., 2009]), to 10^3 m long flow-parallel ridges (termed megascale glacial lineations, MSGLs [*Spagnolo et al*., 2014]) (Figure 1). Subglacial bed forms resist defensible classification, frequently grading together and existing in contrasting form with close proximity, while remaining part of a continuum [*Dowling et al*., 2015; *Ely et al*., 2016]. Much like their aeolian and subaqueous counterparts, subglacial bed forms are likely to develop from a featureless surface without an obvious or plausible pre-existing heterogeneity to control patterning [*Johnson et al*., 2010; *Clark*, 2010]. However, related features can also be seeded by pre-existing topography [*Dowling et al*., 2015]. Despite their ubiquity and centuries of study, no consensus on formative mechanisms or dynamics of subglacial bed forms exists [*Stokes et al*., 2013]. Previous hypotheses on their formation invoke a wide assortment of mechanisms and processes (see discussion in *Menzies* [1979], *Clark* [2010], and *Stokes et al*. [2013]). Their growth and evolution is critical to our understanding of how basal roughness evolves beneath ice sheets [*Schoof*, 2007], and they are likely to influence subglacial hydrological systems and, in turn, ice sheet velocity [*King et al*., 2009; *Sergienko and Hindmarsh*, 2013; *Stokes et al*., 2016]. Moreover, the relationship between basal shear stress and ice velocity has recently been identified as a key uncertainty in attempts to model future ice sheet evolution and concomitant sea level rise [*Ritz et al*., 2015]. As ice sheets play a leading role in climate and sea level change, these findings motivate a general solution to controls on subglacial bed form morphologies and their relationship to the sliding velocity of the overriding ice mass.

Previous work has been dominated by extensive descriptions of sedimentology and morphology (e.g., see reviews in *Menzies* [1979], *Patterson and Hooke* [1995], and *Stokes et al*. [2011]) and, more recently, by analysis of large data sets of bed form morphology [*Dunlop and Clark*, 2006; *Clark et al*., 2009; *Spagnolo et al*., 2014; *Dowling et al*., 2015]. In contrast, modeling [e.g., *Hindmarsh*, 1998; *Pelletier*, 2008; *Chapwanya et al*., 2011; *Hooke and Medford*, 2013; *Fowler and Chapwanya*, 2014] has been less frequently employed. It is difficult to instrument and observe the subglacial environment [cf. *Boulton et al*., 2001], so reductionist-based approaches are constrained by a limited understanding of subglacial physics and enormous parameter uncertainty.

Here we examine the problem with a reduced complexity numerical model. This method uses numerical iteration of simplified mechanisms to unravel mathematical complexity and understand the broad interactions that dominate the development of landforms. Reduced complexity analysis has revolutionized the

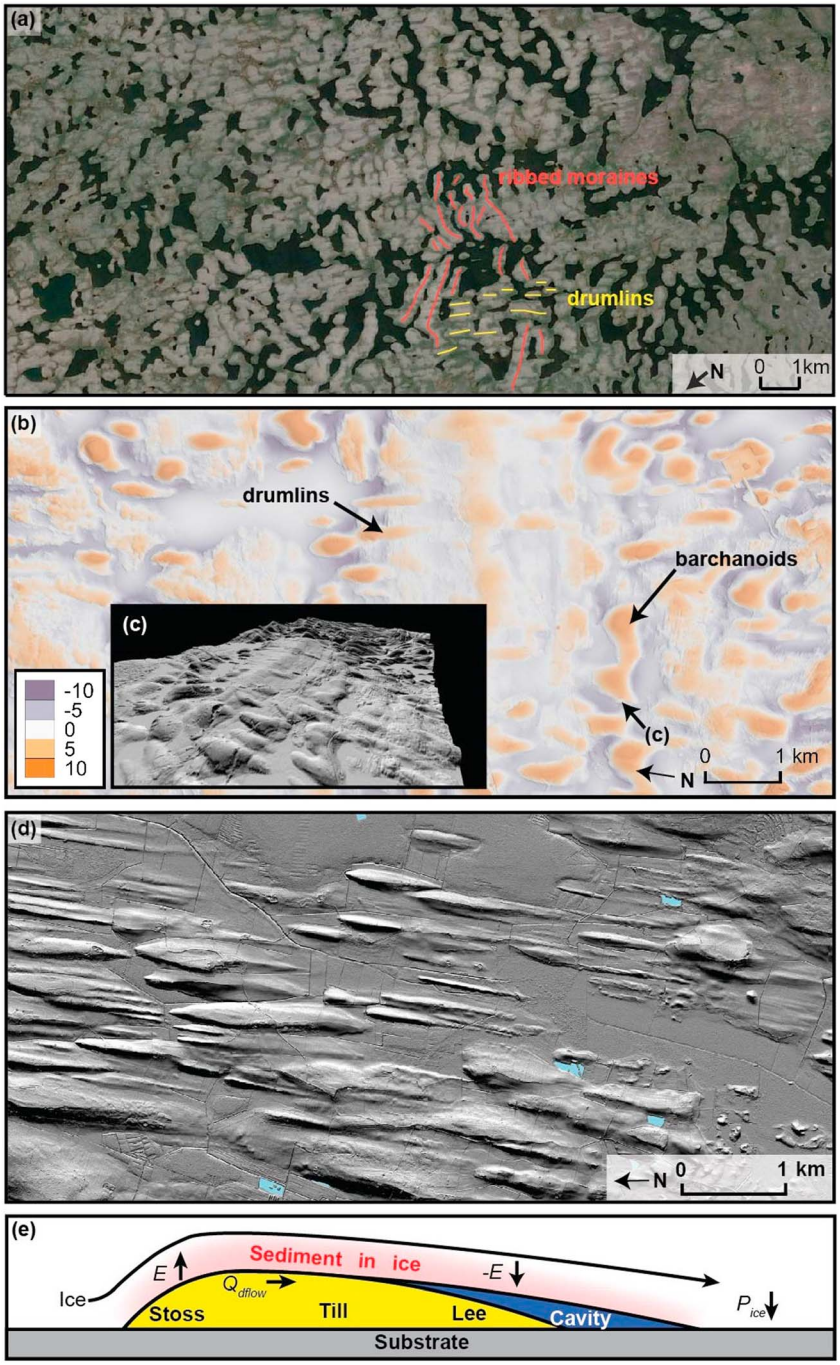

Figure 1. Pleistocene drumlin and ribbed moraine forms in (a) Ennadai Lake, Nunavut, Canada (60.482°N, 101.014°W; data: Google Earth/Landsat), (b, c) Halifax, NS, Canada (inset is oblique vertically exaggerated view from marked point in Figure 1 b), and (d) Hackvad, Sweden (with 5X vertical exaggeration and illumination from the NE, water bodies are in blue). Ice flow is left to right in all panels. Note transitions from ribbed moraine to drumlins and down-flow pattern cloning. Colors in Figure 1c are residual elevations from a 250 m radius mean surface. (e) Profile schematic of the main mechanisms in the model. Ice flow and ice to bed pressure (P_{ice}) drives down-flow till advection (Q_{dflow}). Localized differences in P_{ice} also drive entrainment (E) and deposition ($-E$).

understanding of enigmatic patterned landscapes elsewhere in geomorphology. Many problems where bottom-up reductionist or atemporal analytical methods had only limited success were demonstrated to be the result of simple and widely observed mechanisms iterated through space and time [see *Werner*, 1995, 1999; *Pelletier*, 2008; *Murray et al.*, 2009, 2014]. The appearance of subglacial bed forms is similar to

other patterned landscapes, suggesting such an approach may be productive and complementary to analytically based modeling (see discussion in *Murray et al*. [2009]).

Our approach uses a simple cellular model that emulates several core mechanisms hypothesized to exist subglacially. This study focuses on till-cored bed forms that develop above a hard substrate; we do not treat erosional bed forms in this study [*Stokes et al*., 2011; *Menzies et al*., 2016] (Figure 1). In the model, ice advects down-flow, deforming over topography and applying pressure to the bed. This pressure drives down-flow till flux through bed deformation [*Boulton et al*., 2001; *Schoof*, 2007]. The spatial variability in basal pressure also drives pressure gradient-driven till flux, which advects till from areas of high ice pressure to low ice pressure. Combining and iterating these mechanisms readily produces dune-like bed forms resembling ribbed moraines. However, lee-side deposition is required to elongate ribs into subglacial bed forms [*Anderson*, 2014; *Fowler and Chapwanya*, 2014]. We model this with a mobile sediment load that travels with the ice and entrains or deposits as a function of local pressure. With the addition of this mechanism, drumlins and MSGL readily develop.

We first describe our numerical implementation and then explain how each mechanism contributes to the development of bed form morphology. We then discuss simulation results and experiments constraining the conditions necessary for the formation of various subglacial bed forms. We consider candidate processes for each of the mechanisms and provide estimates of till fluxes. A preliminary phase diagram is developed to relate bed form morphology to ice velocity and sediment thickness.

2. Subglacial Mechanisms and Model Structure

In keeping with the reduced complexity approach, our primary goal is a deep, extensible understanding, rather than precision simulation [*Murray et al*., 2009, 2014]. As such, to limit risk of misparameterization our model deliberately omits detail that is unnecessary. Due to broad uncertainties in the relevant subglacial physics, we model with abstractions and cautiously consider the underlying physical processes.

We iterate mechanisms through time over a raster grid with periodic boundaries (10 m resolution, 400 cells down-flow by 250 cells cross-flow, 0.01 year time step, 500 year simulation length). Initial conditions are a flat bed with defined thickness of till above a nonerodible basement (analogous to a stiff till or bedrock substrate [e.g., *King et al*., 2009; *Boulton et al*., 2001]). The glacier thickness is assumed to be much greater than the bed form heights. By sediment thickness, we mean the total volume of sediment in the model space divided by model space area. This is identical to "equivalent sediment thickness," which exerts a dominating control on aeolian bed form morphology [*Wasson and Hyde*, 1983]. The surface evolution of each cell $\left(\frac{\partial H}{\partial t}\right)$ is broadly

$$\frac{\partial H}{\partial t} = -\frac{\partial Q_{\text{dflow}}}{\partial x} - \frac{\partial Q_{Px}}{\partial x} - \frac{\partial Q_{Py}}{\partial y} - E \tag{1}$$

where Q_{dflow} is the vertically integrated down-flow sediment flux ($\text{m}^3\,\text{m}^{-1}\,\text{yr}^{-1}$), Q_{Px} and Q_{Py} are the pressure gradient-driven vertically integrated sediment flux components ($\text{m}^3\,\text{m}^{-1}\,\text{yr}^{-1}$), x and y are down-flow and cross-flow dimensions, and E is erosion into the ice (where negative E represents deposition from the ice to the bed) ($\text{m}\,\text{yr}^{-1}$). Ice advects from the left with a constant basal speed and thickness and deforms around topography. The pressure exerted on the bed from the ice (P_{ice}, Pa) for each cell is approximated as

$$P_{\text{ice}} = P_g - P_w + v\eta\frac{\partial H}{\partial x} \tag{2}$$

where P_g is the ice pressure from gravity (constant), P_w is the basal water pressure (constant), v is the ice speed at base, η is ice effective viscosity (constant: 10^{14} Pa s, see *Fowler and Chapwanya* [2014] and *Cuffey and Paterson* [2010] for further discussion and specification of subglacial conditions assumed), and $\frac{\partial H}{\partial x}$ is the bed surface slope relative to ice flow (calculated in down-ice direction). If the calculated P_{ice} is negative, the ice base lifts off the bed (a cavity) and $P_{\text{ice}} = 0$. The ice base then sinks toward the bed at a rate of $\frac{-\left(P_g - P_w\right)}{v\eta}$. This core relation controls the length of cavities in the model. Generally, cavities are longer with greater topographic range, faster ice speeds, more viscous ice, greater water pressures, and shallower glacier depths (less P_g). We model Q_{dflow} for each cell with

$$Q_{\text{dflow}} = \min\begin{pmatrix} kP_{\text{ice}} + 0.1rkP_{\text{ice}} \\ 10H \end{pmatrix} \tag{3}$$

where k is a flux control parameter (in $m^3\,m^{-1}\,yr^{-1}\,Pa^{-1}$), r is a uniformly distributed random draw ranging from −0.5 to 0.5, and the 0.1 scales the stochasticity. The minimum in equation (3) pertains to the inability for a flux event to move more sediment than is available at a site. This emulates some unresolved combination of the following mechanisms, all of which are observed to occur subglacially: (i) subglacial till deformation, where till rheology is such that higher P_{ice} leads to greater Q_{dflow} [see *Schoof*, 2007; *Stokes et al*., 2013; *Fowler and Chapwanya*, 2014]; (ii) temporally variable ice-bed coupling [e.g., *Anderson*, 2014]; or (iii) large- or small-scale glaciotectonism or plastic till deformation driven by the down-flow component of P_{ice} as applied to stoss slopes [*Dowling et al*., 2015; *Spagnolo et al*., 2016] (not modeled here but present in reality). The importance of these mechanisms is debated, but all result in some positive relation between down-flow slope and Q_{dflow}, which, regardless of the underlying physics, creates an instability [*Pelletier*, 2008].

Advecting ice creates large spatial differences in P_{ice} that drive pressure gradient-driven sediment flux (Q_P)

$$Q_{Px} = -j\frac{\partial P_{ice}}{\partial x} \tag{4a}$$

$$Q_{Py} = -j\frac{\partial P_{ice}}{\partial y} \tag{4b}$$

where j is a flux control parameter ($m^3\,m^{-1}\,yr^{-1}$ per $Pa\,m^{-1}$). This emulates pressure gradient-driven till deformation, which is distributed to the adjacent four cells. Advecting ice carries significant volumes of sediment, which is entrained into the ice (E) or deposited from the ice ($-E$) with

$$E = b\left(P_{ice} - \left(P_g - P_w\right)\right) \quad \text{if}\left(P_{ice} - \left(P_g - P_w\right)\right) < 0 \tag{5a}$$

$$E = 0.75b\left(P_{ice} - \left(P_g - P_w\right)\right) \quad \textit{if}\left(P_{ice} - \left(P_g - P_w\right)\right) > 0 \tag{5b}$$

where b is a coefficient controlling the erosion rate ($m\,yr^{-1}\,Pa^{-1}$). We generalize the efficacy of erosion processes to a more intuitive form by specifying the rate of sediment deposited in cavities, $E_{cavity} = -b(P_g - P_w)$. The 0.75 creates minor down-ice profile asymmetry [*Spagnolo* et al., 2010] by limiting entrainment on stoss slopes. The physical processes involved with entrainment of sediment are not well understood but are broadly designed here to represent regelation [*Rempel*, 2008] and cavity deposition [*Dardis et al*., 1984]. Although no parameterizations are available, this mechanism has extensive empirical support [*Dardis et al*., 1984; *Möller and Dowling*, 2015; *Stokes et al*., 2011; *Evans et al*., 2015]. Note that to conserve mass in situations with no net erosion of the bed, the erosion and deposition are most plausibly balanced around the static ice pressure ($P_g - P_w$). The processes in equations (4a), (4b), (5a), and (5b) are limited when no sediment is available ($H = 0$).

To relate topography and "feature size," we use metrics quantifying relative "streamlining" and down-ice and cross-ice feature dimensions, measured along transects. Feature dimensions (morphology) provide some commensurability with empirical measurements [e.g., *Dowling et al*., 2015]. We avoid "bed form polygon" methods and automated shape metrics to limit ambiguity in transitional bed form types, ensure transparency, facilitate large-scale automation, and limit influence from poorly understood and widely discussed subjectivities [*Hillier et al*., 2015]. Relative streamlining (s) of a landscape is evaluated with

$$s = \frac{\sum|\cos(a)|}{\left(\sum|\cos(a)| + \sum|\sin(a)|\right)} \tag{6}$$

where a is the local aspect of each cell (ice flow from the left), and $|\,|$ indicates absolute value. This quantifies the relative distribution of aspects in the landscape: $s = 0.5 \approx$ conical hill, $s < 0.5 \approx$ flow-perpendicular ridges, and $s > 0.5 \approx$ flow-parallel ridges ("streamlined") [*Ely et al*., 2016]. Row and column transects were used to develop feature size estimates. A feature cell was defined where elevation is greater than mean elevation. The length of each segment of consecutive feature cells (considering periodic boundaries) along rows or columns created a population of feature length and width estimates, respectively. To relate mean dimension determined through a population of feature transect lengths to classical bed form polygon lengths derived from bounding box dimensions [e.g., *Clark et al*., 2009; *Dowling et al*., 2015], we assumed ovoid feature shape and multiplied each reported mean dimension by $\frac{4}{\pi}$.

We detail parameters for simulations described in section 3 here, with the exception of parameters that vary as part of ensembles. Parameters common to all simulations: $P_g - P_w = 5.0 \times 10^6$ Pa, $\eta = 3.17 \times 10^6$ Pa yr, and

$k = 2.0 \times 10^6\ \mathrm{m^3\ m^{-1}\ yr^{-1}\ Pa^{-1}}$. Simulations in Figure 2 are part of Ensemble 1. We report all results at 500 years to represent a "mature form," although the primary morphologies develop over shorter timescales.

3. Simulations and Discussion

3.1. Bed Form Development and Dynamics

Iteration of the above mechanisms readily creates bed forms with salient characteristics similar to classic subglacial bed forms, from ribbed moraine (Figure 2a) to drumlins (Figure 2b) to elongate drumlins/MSGLs (Figure 2c). The primary driver of form variability is ice speed, which is consistent with empirical results [*King et al*., 2009]. The bed forms migrate down-flow on the substrate and the broad pattern characteristics stabilize after ≈ 200 years, both of which are typical for bed forms [*Murray et al*., 2014]. There are notable parallels between the subglacial bed forms modeled here and subaqueous or aeolian bed forms, in both driving mechanisms and dynamics.

While the physics that occur subglacially are very different from other environments with bed forms, the abstractions of those physics are similar. First, any positive relation between Q_{dflow} and down-flow bed slope readily creates bumps that self-amplify in the flow field. For example, this is the case for the aerodynamic and screening instabilities in aeolian bed forms, which yield a similar positive relation [see *Kok et al*., 2012]. Second, the development of cavities in the lee of bed forms is similar to the lee-side separation cell and sets up a nearly analogous down-flow length scale for ribbed moraines. Note that lee separation cells (or cavities) alone create sufficiently potent down-flow differences in Q_{dflow} to maintain bed forms, even without any additional flux/slope dependencies ($Q_{\mathrm{dflow}} = 0$ in cavities, $Q_{\mathrm{dflow}} > 0$ elsewhere) [e.g., *Werner*, 1995]. Third, some lateral flux is necessary to connect topography cross-flow. In aeolian and subaqueous bed forms, this is accomplished with some combination of repose, fluid steering, direction variability, and particle diffusion (see review in *Rubin* [2012]). Here we explicitly parameterize this as a function of P_{ice} gradients. Erosion and advection of sediment in the ice is directly analogous to aeolian bed forms where the advection length of particles is similar to bed form dimensions. In aeolian dunes, this is sometimes referred to as "modified suspension" [*Kok* et al., 2012]. This mechanism is comparatively much more effective in subglacial bed forms and is responsible for elongate lee tails in drumlins and MSGLs, places where avalanches or grain fall would dominate in aeolian and subaqueous bed forms.

Very broadly, the dynamics of our modeled subglacial bed forms are similarly analogous. Ribbed moraines are analogous to transverse bed forms, and drumlins and MSGLs are analogous to barchans. Note that the analogy between barchans and drumlins and MSGLs is not in morphology, but in the broad behavioral class of bed forms that are as follows: (i) supply limited by substrate, (ii) self-maintaining, and (iii) not linked to adjacent forms cross-flow [see *Kocurek et al*., 2010].

In more detail, the dynamics of ribbed moraine development is similar to that of transverse dunes. The dependency between pressure and flux creates bumps that amplify in height. The cross-flow flux links incipient bumps into cross-ice bed forms [*Werner*, 1995; *Rubin*, 2012], and the lee cavity size exerts a dominating spacing control. The spacing of ribbed moraines should scale with $\frac{\nu\eta}{(P_g - P_w)}$ multiplied by bed form height [cf. *Nye*, 1953], similar to the manner in which the lee separation cell controls aeolian bed form spacing and collision dynamics [*Kocurek et al*., 2010; *Hugenholtz and Barchyn*, 2012]. These characteristics are widely observed in real ribbed moraines, where consistent spacing yields down-ice pattern cloning [*Dunlop and Clark*, 2006]. Much like other bed forms, ribbed moraine size self-organizes and patterns mature due to two feedbacks: (i) sediment bleed from crestline lateral edges reduces the length of short crests, preferentially leading to the demise of short crestlines, and (ii) smaller bed forms have faster celerity and thus collide with larger features, increasing and homogenizing size [*Kocurek et al*., 2010].

Increasing ice speed creates more elongate bed forms (drumlins and MSGL, Figures 2b and 2c) for a variety of reasons. First, in the simulations increasing ice speed creates significantly more stoss pressure on bumps in the bed as ice is forced to deform at a faster rate. This translates to greater spatial variability in Q_{dflow}, accelerating bed form development and amplifying differences in incipient proto-bed form celerities. Second, lee tails elongate due to larger lee-side cavities and greater flux of sediment entrained in the ice (because of faster ice speed). Third, locking sediment in lee tails has a similar effect to reducing total sediment

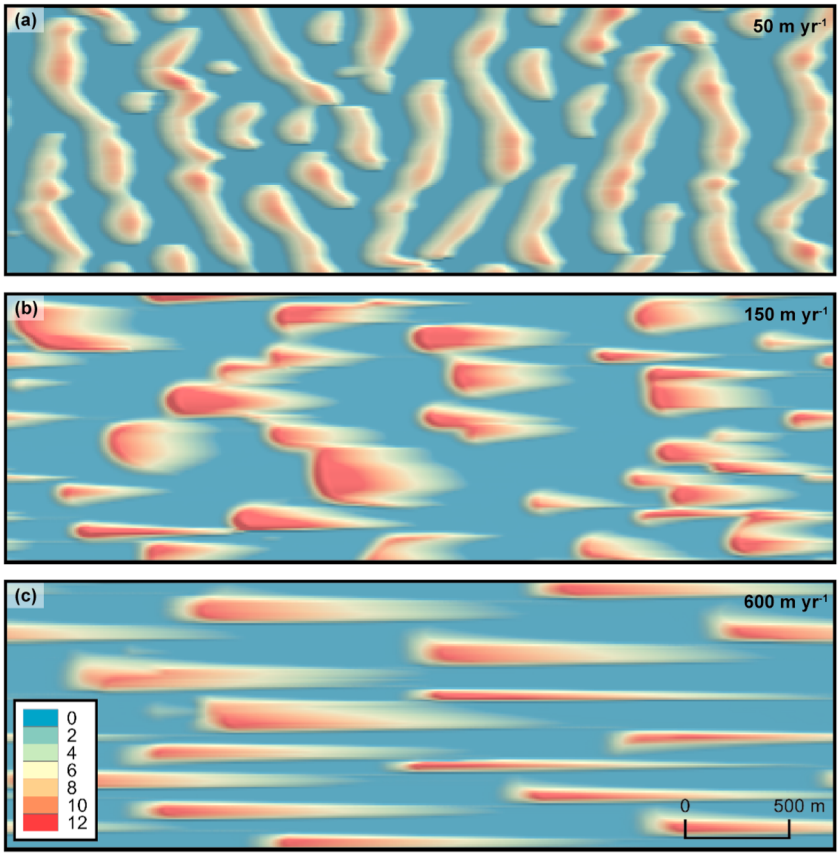

Figure 2. Sample model outputs that resemble (a) ribbed moraine, (b) drumlins, (c) and megascale glacial lineations after 500 years. These simulations were taken from Ensemble 1 (see Figure 3). Note barchanoid ribbed moraine features and classical bed form pattern cloning in Figure 2a. The transition between Figures 2a and 2b is sharp in the phase space, as lateral linking breaks up, the morphology trends toward discrete forms. Videos of simulations with the parameters used above are available in the supporting information or online: Movie S1, https://youtu.be/2RP-NjgcQ18 (Figure 2a); Movie S2, https://youtu.be/sTRXHGYq5Rk (Figure 2b); and Movie S3, https://youtu.be/DpqVp0ZXqYc (Figure 2c).

thickness. Sediment thickness exerts a dominating control on the transition from transverse features (ribbed moraines) to isolated features as in aeolian dunes [*Werner*, 1995]. In combination, these effects increase spacing, bed form length, and restrict bed form lateral linking.

Increasing ice speed further creates longer and more streamlined bed forms (Figures 2b and 2c) that trend toward features that might be described as MSGLs. In reality, ice streams are characterized by both low P_{ice} and high ice speeds, both of which force elongation by extending cavities and low-pressure lee areas. This provides an explanation for the positive relation between feature elongation and ice speed, empirically observed [*King et al.*, 2009] but not resolved mechanistically.

3.2. Bed Form Feedback Moderation and Sediment Thickness

The modeled bed forms are driven by an amplifying feedback (positive dependency between P_{ice} and Q_{dflow}) but are moderated by (i) pressure gradient-driven flux, which advects sediment from incipient bumps cross-ice, and (ii) entrainment, which reduces stoss pressure by entraining sediment into the ice and advecting it over the incipient forms. We use Ensemble 1 to explore variation in moderation mechanisms (Figures 3a, 3c, and 3e). Ensemble 1 used an initial sediment thickness of 5 m; other parameters are specified in Figure 3 or section 2.

Varying the dominant moderation mechanism from entrainment (left side of Figures 3a, 3c, and 3e) to pressure gradient-driven flux (right side) constrains an estimate of fluxes. Simulations moderated dominantly through entrainment tend to wash out features and promote shallow stoss slopes (entrainment removes sediment from stoss to moderate pressures). Contrarily, simulations moderated dominantly through pressure

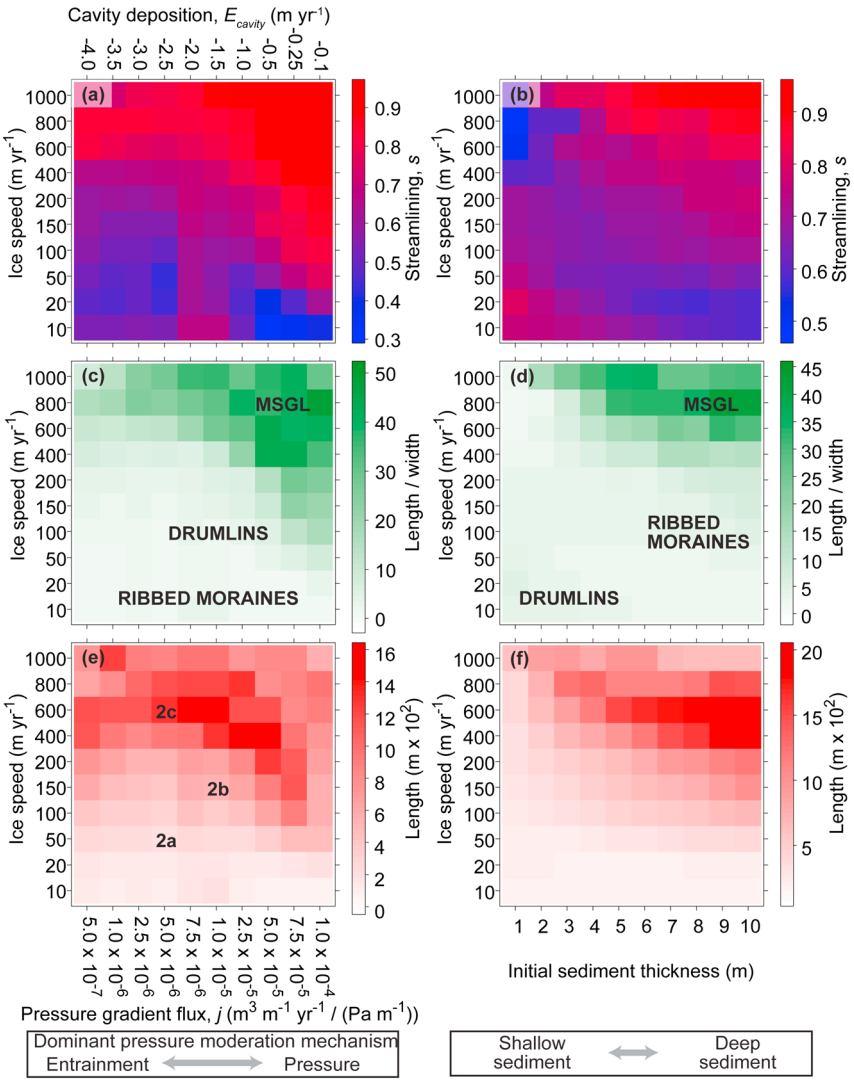

Figure 3. Ensemble simulation raster plots demonstrating the results of (a, c, and e) varying ice speed versus pressure gradient-driven flux and entrainment (Ensemble 1, left side) and (b, d, and f) varying ice speed versus initial sediment depth (Ensemble 2, right side). Each cell is colored to describe the topography with streamlining (Figures 3a and 3b; see equation (2)), feature length/width ratio (Figures 3c and 3d), and feature length (Figures 3e and 3f). Ensemble 1 demonstrates the effect of varying the pressure moderation mechanism, from entrainment dominated (left side) to pressure gradient-driven flux dominated (right side). Ensemble 2 demonstrates the effect of varying the initial sediment depth from conditions with little sediment (left side) to those with abundant sediment. Approximate bed form types are annotated in Figures 3c and 3d, and the simulations shown in Figures 2a–2c are marked in Figure 3e.

gradient-driven flux have blunt stoss slopes, which accelerate amplification, drive differences in celerity, and lead to MSGL-type bed forms (see supporting information Movies S1–S3). Ensemble 1 constrains the most likely values to those characterized by properties in the center of the figure.

In Ensemble 2 (Figures 3b, 3d, and 3e) we explore the implications of limiting sediment available for transport through initial sediment depth (note that sediment is conserved and boundaries are periodic). Parameters specific to Ensemble 2 are $j = 2.52 \times 10^{-6}\,\mathrm{m^3\,m^{-1}\,yr^{-1}/(Pa\,m^{-1})}$ and $E_{\mathrm{cavity}} = -2\,\mathrm{m\,yr^{-1}}$ (see section 2 for other parameters). At low ice speeds ($<200\,\mathrm{m\,yr^{-1}}$), features are small and not particularly streamlined. Increasing sediment thickness prompts an increase in lateral connectivity as features are more closely spaced and more likely to succumb to linking feedbacks [*Rubin*, 2012]—more sediment prompts development of ribbed moraines under identical ice speed. At higher ice speeds ($>100\,\mathrm{m\,yr^{-1}}$), the larger features are greater in amplitude and longer, restricting lateral linking by increasing spacing. The longest and most streamlined

features are associated with relatively abundant sediment (Figure 3d). These simulations suggest that some transitions in bed form type that occur in close proximity [*Trommelen et al*., 2014] may be driven by differences in the thickness of sediment.

Generally, Figure 3 provides some initial parameterization of a phase space that may be used to invert paleolandscapes (similar to *Southard and Boguchwal* [1990]), which is a potentially powerful advance. However, note that these are tentative results due to the broad uncertainty in underlying physical mechanisms.

3.3. Subglacial Processes and Sedimentology

Encouragingly, this model simulates bed forms that emulate reality, but it is highly abstracted due to lack of understanding of the relevant physics. Ice behavior is modeled in a simplified manner, primarily for computational efficiency. Nevertheless, the model emulates the broad patterns of P_{ice} expected to occur subglacially. In addition, the underlying processes responsible for Q_{dflow} require resolution. The most likely constituent of Q_{dflow} is till deformation [*Boulton et al*., 2001]. Predicted till fluxes of $2.0 \times 10^{-6}\,m^3\,m^{-1}\,yr^{-1}\,Pa^{-1}$ (Figure 2b) represent $10\,m^3\,m^{-1}\,yr^{-1}$ at $(P_g - P_w) = 5.0 \times 10^6$ Pa, which is similar but perhaps an underestimate compared with values from *Boulton et al*. [2001]. However, note that till deformation is not the only possible mechanism that could produce bed forms through an instability (see section 2).

Pressure gradient-driven till flux is not widely discussed in the literature, but without some form of lateral connectivity, topography would have unrealistically sharp cross-ice elevation differences [*Rubin*, 2012]. We do not ascribe a specific process to pressure gradient-driven till flux, but it could be a combination of ice deflection and water-driven sediment flux. Deflection of clast fabrics supports the presence of lateral sediment advection [e.g., *Stokes et al*., 2011, Figure 15].

This model predicts bed forms to be filled with deposition facies from down-flow till advection, distrainment, and lateral flux (near edges of cavities). This facies assemblage is not particularly discriminatory and generally matches the sedimentology of shallow sediment bed forms [*Stokes et al*., 2011; *Evans et al*., 2015; *Menzies et al*., 2016; *Spagnolo et al*., 2016].

4. Conclusions and Implications

This model suggests that subglacial bed form dynamics largely mirror those in fluvial or aeolian domains despite the difference in the properties of the fluid involved. Although the driving physics are different, abstractions of the physics are similar. Moreover, the simulations provide further evidence that ribbed moraines, drumlins, and MSGL in shallow sediments are likely to form from the same mechanisms, which is consistent with recent studies based only on morphology [cf. *Ely et al*., 2016]. Ice speed and cavity length (as a proxy for lee low pressure) appear to control elongation, a hypothesis widely discussed but not yet linked mathematically [*Spagnolo et al*., 2014]. Furthermore, these simulations have generated several hypotheses to be tested. (i) Ribbed moraine spacing should scale with an ice cavity collapse length scale, much like transverse dune spacing is controlled by lee separation cell dimensions [*Kocurek et al*., 2010]. (ii) Sediment thickness should exert a controlling influence on bed form morphology (see Figure 3). (iii) Till flux estimates (see Figure 3) can be readily compared to empirical estimates but should be explored with more sophisticated analytical modeling and laboratory experiments. (iv) The treatment of subglacial bed forms as classical bed forms opens the possibility of using classical bed form pattern metrics [*Kocurek et al*., 2010] to assess to complex ice flow histories.

Acknowledgments

Code to reproduce this paper and all simulation data are available by request to T.E.B. or at https://github.com/tbarchyn/STAB_1.0. Data in Figure 1a are available from Google Earth (http://earth.google.ca). Data in Figures 1b and 1c are available from http://halifax.ca/opendata. The LiDAR data used to generate the hillshade model in Figure 1d are the property of Lantmäteriet and are used free at the point of demand through funding provided by the Research Council of Sweden (http://www.geodata.se/sv/Ga-med/Forskning-utbildning-och-kulturverksamhet/), under agreement l2014/00579. This research was enabled by computing resources provided by Westgrid and Compute Canada/Calcul Canada. We gratefully acknowledge project funding from the University of Calgary, Lund University, and Durham University. We also thank Andrew Fowler for comments on a previous draft and Bob Anderson and Andy Wickert for comprehensive reviews that led to major improvements.

References

Anderson, R. S. (2014), Evolution of lumpy glacial landscapes, *Geology*, *42*, 679–682, doi:10.1130/G35537.1.

Boulton, G. S., K. E. Dobbie, and S. Zatsepin (2001), Sediment deformation beneath glaciers and its coupling to the subglacial hydraulic system, *Quat. Int.*, *86*, 3–28, doi:10.1016/S1040-6182(01)00048-9.

Chapwanya, M., C. D. Clark, and A. C. Fowler (2011), Numerical computations of a theoretical model of ribbed moraine formation, Earth Surf, *Proc. Land.*, *36*, 1105–1112, doi:10.1002/esp.2138.

Clark, C. D. (2010), Emergent drumlins and their clones: From till dilatancy to flow instabilities, *J. Glaciol.*, *51*, 1011–1025, doi:10.3189/002214311796406068.

Clark, C. D., A. L. C. Hughes, S. L. Greenwood, M. Spagnolo, and F. S. L. Ng (2009), Size and shape characteristics of drumlins, derived from large sample, and associated scaling laws, *Quat. Sci. Rev.*, *28*, 677–692, doi:10.1016/j.quascirev.2008.08.035.

Cuffey, K. M., and W. S. B. Paterson (2010), *The Physics of Glaciers*, Butterwork-Heinemann, Burlington, Mass.

Dardis, G. F., A. M. McCabe, and W. I. Mitchell (1984), Characteristics and origins of lee-side stratification sequences in late Pleistocene drumlins, Northern Ireland, *Earth Surf. Proc. Land.*, *9*, 409–424, doi:10.1002/esp.3290090503.

Dowling, T. P. F., M. Spagnolo, and P. Möller (2015), Morphometry and core type of streamlined bedforms in southern Sweden from high resolution LiDAR, *Geomorphology*, *236*, 54–63, doi:10.1016/j.geomorph.2015.02.018.
Dunlop, P., and C. D. Clark (2006), The morphological characteristics of ribbed moraine, *Quat. Sci. Rev.*, *25*, 1668–1691, doi:10.1016/j.quascirev.2006.01.002.
Ely, J. C., C. D. Clark, M. Spagnolo, C. R. Stokes, S. L. Greenwood, A. L. C. Hughes, P. Dunlop, and D. Hess (2016), Do subglacial bedforms comprise a size and shape continuum?, *Geomorphology*, *257*, 108–119, doi:10.1016/j.geomorph.2016.01.001.
Evans, D. J. A., D. H. Roberts, and C. Ó. Cofaigh (2015), Drumlin sedimentology in a hard-bed, lowland setting, Connemara, western Ireland: Implications for subglacial bedform generation in areas of sparse till cover, *J. Quaternary Sci.*, *30*, 537–557, doi:10.1002/jqs.2801.
Fowler, A. C., and M. Chapwanya (2014), An instability theory for the formation of ribbed moraine, drumlins and mega-scale glacial lineations, *Proc. Royal Soc. A*, *470*, 20,140,185, doi:10.1098/rspa.2014.0185.
Hillier, J. K., et al. (2015), Manual mapping of drumlins in synthetic landscapes to assess operator effectiveness, *J. Maps*, *11*, doi:10.1080/17445647.2014.957251.
Hindmarsh, R. C. A. (1998), The stability of a viscous till sheet coupled with ice flow, considered at wavelengths less than the ice thickness, *J. Glaciol.*, *44*, 285–292.
Hooke, R. L., and A. Medford (2013), Are drumlins a product of a thermo-mechanical instability?, *Quat. Res.*, *79*, 458–464, doi:10.1016/j.yqres.2012.12.002.
Hugenholtz, C. H., and T. E. Barchyn (2012), Real barchan dune collisions and ejections, *Geophys. Res. Lett.*, *39*, L02306, doi:10.1029/2011GL050299.
Johnson, M. D., A. Schomacker, I. Örn Benediktsson, A. J. Geiger, A. Ferguson, and O. Ingólfsson (2010), Active drumlin field revealed at the margin of Múlajökull, Iceland: A surge-type glacier, *Geology*, *38*, 943–946, doi:10.1130/G31371.1.
King, E. C., R. C. A. Hindmarsh, and C. R. Stokes (2009), Formation of mega-scale glacial lineations observed beneath a West Antarctic ice stream, *Nat. Geosci.*, *2*, 585–588, doi:10.1038/ngeo581.
Kocurek, G., R. C. Ewing, and D. Mohrig (2010), How do bedform patterns arise? New views on the role of bedform interactions within a set of boundary conditions, *Earth Surf. Proc. Land.*, *35*, 51–63, doi:10.1002/esp.1913.
Kok, J. F., E. J. R. Parteli, T. I. Michaels, and D. Bou Karam (2012), The physics of wind-blown sand and dust, *Rep. Prog. Phys.*, *75*, 106901, doi:10.1088/0034-4885/75/10/106901.
Menzies, J. (1979), A review of the literature on the formation and location of drumlins, *Earth Sci. Rev.*, *14*, 315–359, doi:10.1016/0012-8252(79)90093-X.
Menzies, J., D. P. Hess, J. M. Rice, K. G. Wagner, and E. Ravier (2016), A case study in the New York Drumlin Field, an investigation using microsedimentology, resulting in refinement of a theory of drumlin formation, *Sedimentary Geol.*, doi:10.1016/j.sedgeo.2016.01.017, in press.
Möller, P., and T. P. F. Dowling (2015), The importance of thermal boundary transitions on glacial geomorphology: Mapping of ribbed/hummocky moraine and streamlined terrain from LiDAR, over Småland, South Sweden, *GFF*, *137*(4), 452–283, doi:10.1080/11035897.2015.1051736.
Murray, A. B., et al. (2009), Geomorphology, complexity, and the emerging science of the Earth's surface, *Geomorphology*, *103*, 496–505, doi:10.1016/j.geomorph.2008.08.013.
Murray, A. B., E. B. Goldstein, and G. Coco (2014), The shape of patterns to come: From initial formation to long-term evolution, *Earth Surf. Proc. Land.*, *39*, 62–70, doi:10.1002/esp.3487.
Nye, J. F. (1953), The flow law of ice from measurements in glacier tunnels, laboratory experiments and the Jungfraufirn Borehole Experiment, *Proc. Roy. Soc. Lond. Math. Phys. Sci.*, *219*, 477–489.
Patterson, C. J., and L. H. Hooke (1995), Physical environment of drumlin formation, *J. Glaciol.*, *41*, 30–38.
Pelletier, J. D. (2008), *Quantitative Modeling of Earth Surface Processes*, Cambridge Univ. Press, Cambridge, U. K.
Rempel, A. W. (2008), A theory for ice-till interactions and sediment entrainment beneath glaciers, *J. Geophys. Res.*, *113*, F01013, doi:10.1029/2007JF000870.
Ritz, C., T. L. Edwards, G. Durand, A. J. Payne, V. Peyaud, and R. C. A. Hindmarsh (2015), Potential sea-level rise from Antarctic ice-sheet instability constrained by observations, *Nature*, *528*, 115–118, doi:10.1038/nature16147.
Rubin, D. M. (2012), A unifying model for planform straightness of ripples and dunes in air and water, *Earth Sci. Rev.*, *113*, 176–185, doi:10.1016/j.earscirev.2012.03.010.
Schoof, C. (2007), Pressure-dependent viscosity and interfacial instability in coupled ice-sediment flow, *J. Fluid Mech.*, *570*, 227–252, doi:10.1017/S0022112006002874.
Sergienko, O. V., and R. C. A. Hindmarsh (2013), Regular patterns in frictional resistance of ice-stream beds seen by surface data inversion, *Science*, *342*, 1086–1089, doi:10.1126/science.1243903.
Southard, J. B., and L. A. Boguchwal (1990), Bed configurations in steady unidirectional water flows: Part 2. Synthesis of flume data, *J. Sed. Petrology*, *60*, 658–679.
Spagnolo, M., C. D. Clark, A. L. C. Hughes, and P. Dunlop (2010), The topography of drumlins; Assessing their long profile shape, *Earth Surf. Proc. Land.*, *36*, 790–804, doi:10.1002/esp.2107.
Spagnolo, M., C. D. Clark, J. C. Ely, C. R. Stokes, J. B. Anderson, K. Andreassen, A. G. C. Graham, and E. C. King (2014), Size, shape and spatial arrangement of mega-scale glacial lineations from a large and diverse dataset, *Earth Surf. Proc. Land.*, *39*, 1432–1448, doi:10.1002/esp.3532.
Spagnolo, M., et al. (2016), Ice stream motion facilitated by a shallow-deforming and accreting bed, *Nature Comm.*, *7*, 10,723, doi:10.1038/ncomms10723.
Stokes, C. R., M. Spagnolo, and C. D. Clark (2011), The composition and internal structure of drumlins: Complexity, commonality, and implications for a unifying theory of their formation, *Earth Sci. Rev.*, *107*, 398–422, doi:10.1016/j.earscirev.2011.05.001.
Stokes, C. R., A. C. Fowler, C. D. Clark, R. C. A. Hindmarsh, and M. Spagnolo (2013), The instability theory of drumlin formation and its explanation of their varied composition and structure, *Quat. Sci. Rev.*, *62*, 77–96, doi:10.1016/j.quascirev.2012.11.011.
Stokes, C. R., M. Margold, C. D. Clark, and L. Tarasov (2016), Ice stream activity scaled to ice sheet volume during Laurentide Ice Sheet deglaciation, *Nature*, *530*, 322–326, doi:10.1038/nature16947.
Trommelen, M. S., M. Ross, and A. Ismail (2014), Ribbed moraines in northern Manitoba, Canada: Characteristics and preservation as part of a subglacial bed mosaic near the core regions of ice sheets, *Quat. Sci. Rev.*, *87*, 135–155, doi:10.1016/j.quascirev.2014.01.010.
Wasson, R. J., and R. Hyde (1983), Factors determining desert dune type, *Nature*, *304*, 337–339.
Werner, B. T. (1995), Eolian dunes: Computer simulations and attractor interpretation, *Geology*, *23*, 1107–1110.
Werner, B. T. (1999), Complexity in natural landform patterns, *Science*, *284*, 102–104, doi:10.1126/science.284.5411.102.